Mon. Not. R. Astron. Soc. **344,** 965–977 (2003)

Fundamental parameters of the LMC clusters NGC 1836, NGC 1860, NGC 1865, SL 444, LW 224 and SL 548

Andrés E. Piatti,[1⋆] Eduardo Bica,[2⋆] Doug Geisler[3⋆] and Juan J. Clariá[4⋆]

[1]*Instituto de Astronomía y Fisica del Espacio, CC 67, Suc. 28, 1428, Capital Federal, Argentina*
[2]*Universidade Federal do Rio Grande do Sul, Depto. de Astronomía, CP 15051, Porto Alegre, 91500-970, Brazil*
[3]*Universidad de Concepción, Departamento de Física, Casilla 160-C, Concepción, Chile*
[4]*Observatorio Astronómico, Laprida 854, 5000 Córdoba, Argentina*

Accepted 2003 June 4. Received 2003 May 30; in original form 2003 March 11

ABSTRACT

Complementing our recent Washington photometric studies on intermediate age and young Large Magellanic Cloud (LMC) clusters, we now turn our attention to six previously unstudied star clusters in the transition range 200–700 Myr. We study NGC 1836, 1860 and 1865, which are projected on the LMC bar; SL 444, also located in the central disc but outside the bar; and LW 224 and SL 548, both located in the outer disc. We derive ages and metallicities from extracted T_1 versus $C–T_1$ colour–magnitude diagrams (CMDs), using theoretical isochrones recently computed for the Washington photometric system. For the metallicity determinations, these CMDs are particularly sensitive. We also estimate ages and metallicities of the surrounding fields of NGC 1860 and 1865 by employing the δT_1 index defined in Geisler et al. (1997, AJ, 114, 1920) and theoretical isochrones. By adding the present cluster sample to those of our previous studies, we now gather 37 LMC clusters with homogeneous parameter determinations, which are employed to probe the chemical enrichment of the LMC and its spatial distribution. On average, inner disc clusters turned out to be not only younger than the outer ones, but also more metal-rich; some have solar metal content. Furthermore, inner clusters located to the west of the LMC centre are younger and more metal-rich than their eastern counterparts. We propose that a bursting formation mechanism, with an important formation event centred at ∼2.0 Gyr, provides a better description of the cluster age–metallicity relation than a closed-box chemical evolution model. In the outer disc, the field star formation seems to have lasted until 2 Gyr ago while it continued in the inner disc for almost 1 Gyr longer.

Key words: techniques: photometric – galaxies: individual: Large Magellanic Cloud – Magellanic Clouds – galaxies: star clusters.

1 INTRODUCTION

The Magellanic Clouds and our own Galaxy form part of a Local Group of some 40 galaxies, the total extent of which is about 2 Mpc (Mateo 1998). Except the Sagittarius dwarf galaxy (Ibata, Gilmore & Irwin 1994), the Large (LMC) and Small (SMC) Magellanic Clouds are the two nearest galaxies to our own. For this reason, they are highly desirable to test the theories of stellar and Galactic evolution. In particular, star clusters in the LMC can facilitate our understanding of the chemical enrichment and star-formation history of the galaxy as a whole (Rich, Shara & Zurek 2001; Piatti et al. 2002). Unfortunately, the well-known pronounced cluster age gap from ∼3 to 9 Gyr (e.g. Geisler et al. 1997) does not allow us to use them in order to learn the chemical enrichment and star-formation history of the LMC in detail during this long period of quiescence. In order to thoroughly know how cluster age and metal abundance correlate in the periods during which there was star formation in the LMC, it is necessary to determine reliable ages and metallicities for a large number of star clusters.

The present study deals with Washington photometry of six unstudied star clusters located in two different regions of the LMC. This represents the continuation of a systematic study of LMC clusters carried out as uniformly as possible using the same telescope, detector and the Washington photometric system (Geisler et al. 1997; Bica et al. 1998; Piatti et al. 2002; Geisler et al. 2003; Piatti et al. 2003). Our objective consists of deriving ages and metallicities for these six star clusters and to combine these results with those obtained in our previous studies of the LMC using the same technique. In some cases, we have been able to continue our related studies of the field populations surrounding LMC clusters. The reasons why

⋆E-mail: andres@iafe.uba.ar (AEP); bica@if.ufrgs.br (EB); doug@kukita.cfm.udec.cl (DG); claria@mail.oac.uncor.edu (JJC)

we have chosen to work in this photometric system, and the advantages this represents for this type of study, have already been described in previous works (e.g., Geisler et al. 1997; Piatti et al. 2003). Using a sample of 37 LMC clusters with parameters determined homogeneously we re-examine the relation between the ages and metallicities of the LMC clusters by comparing the results obtained with theoretical predictions.

The cluster sample is described in Section 2. The construction of optimum colour–magnitude diagrams (CMDs) is presented in Section 3. Ages and metallicities for the present cluster sample are derived in Section 4. In Section 5 we examine the ages and metallicities of a total of 37 LMC clusters, which have been studied up to the present using the same technique, to probe the chemical enrichment of the LMC and its spatial distribution. The main conclusions of this work are summarized in Section 6.

2 THE DATA

Most of the present clusters (Table 1) were serendipitously observed in the fields of other target clusters centred in a given frame. One

Table 1. Object list.

Cluster[a]	α_{2000} (h m s)	δ_{2000} (° ′ ″)	ℓ (°)	b (°)	Reference field
NGC 1836, SL 223, ESO 56-SC31, BRHT4a	05 05 35	−68 37 42	279.5	−34.7	SL 244
NGC 1860, SL 284, ESO 56-SC75	05 10 39	−68 45 14	279.6	−34.2	NGC 1865
NGC 1865, SL 307, ESO 56-SC78	05 12 25	−68 46 23	279.5	−34.0	NGC 1865
SL 444, KMHK 861	05 24 30	−67 40 41	278.0	−33.2	SL 446A
SL 446, KMHK 869	05 24 47	−67 43 32	278.0	−33.1	SL 446A
LW 224	05 29 56	−72 03 17	283.0	−31.9	SL 555
SL 548, LW 235, KMHK 1035	05 31 24	−72 02 33	283.0	−31.8	SL 555

Note: [a]cluster identifications are from Shapley & Lindsay (1963, SL), Lyngå & Westerlund (1963, LW), Lauberts (1982, ESO), Kontizas et al. (1990, KMHK) and Bhatia et al. (1991, BRHT).

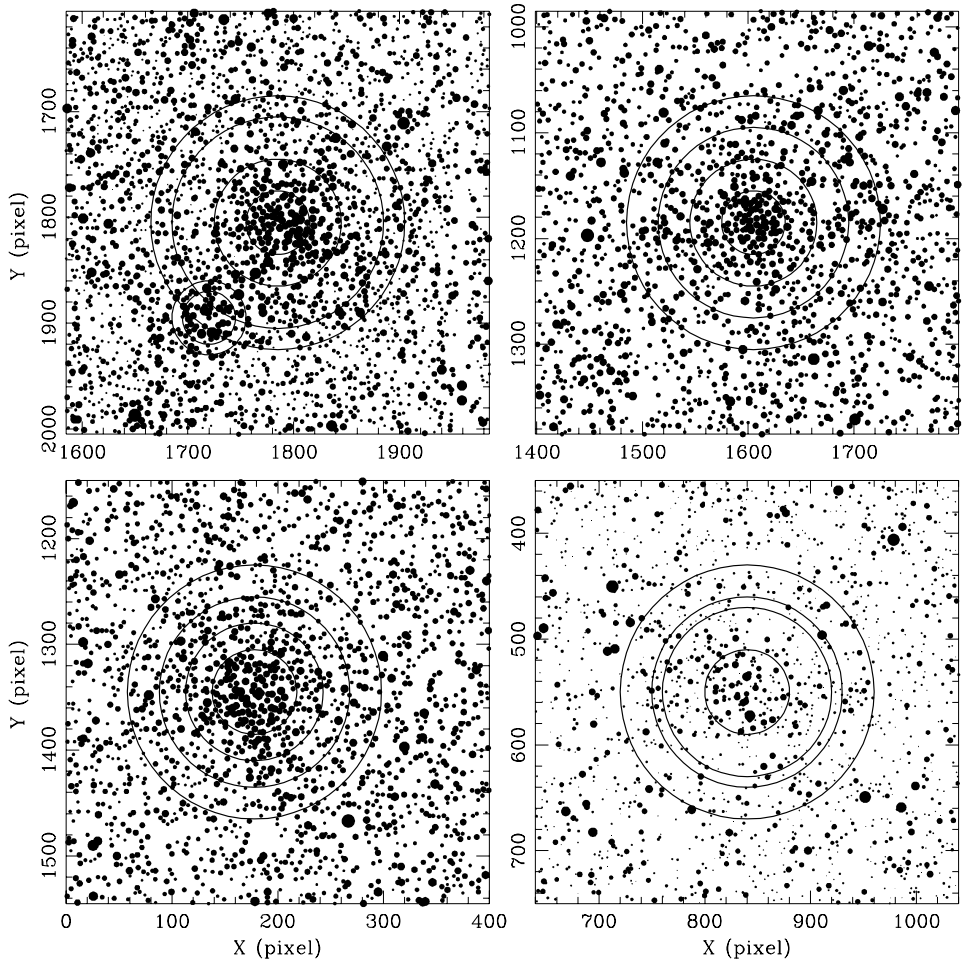

Figure 1. Schematic finding charts for the studied LMC cluster fields are shown as follows. This page; NGC 1836 centred (top left-hand panel; the cluster located to the south-east from NGC 1836 is BRHT4b, see Piatti et al. 2003), NGC 1860 (top right-hand panel), NGC 1865 (bottom left-hand panel), and SL 444 (bottom right-hand panel). Next page; SL 446 (top left-hand panel), LW 224 (top right-hand panel) and SL 548 (bottom panel). Four circular extractions are shown. North is up and east is to the left. The sizes of the plotting symbols are proportional to the T_1 brightness of the star.

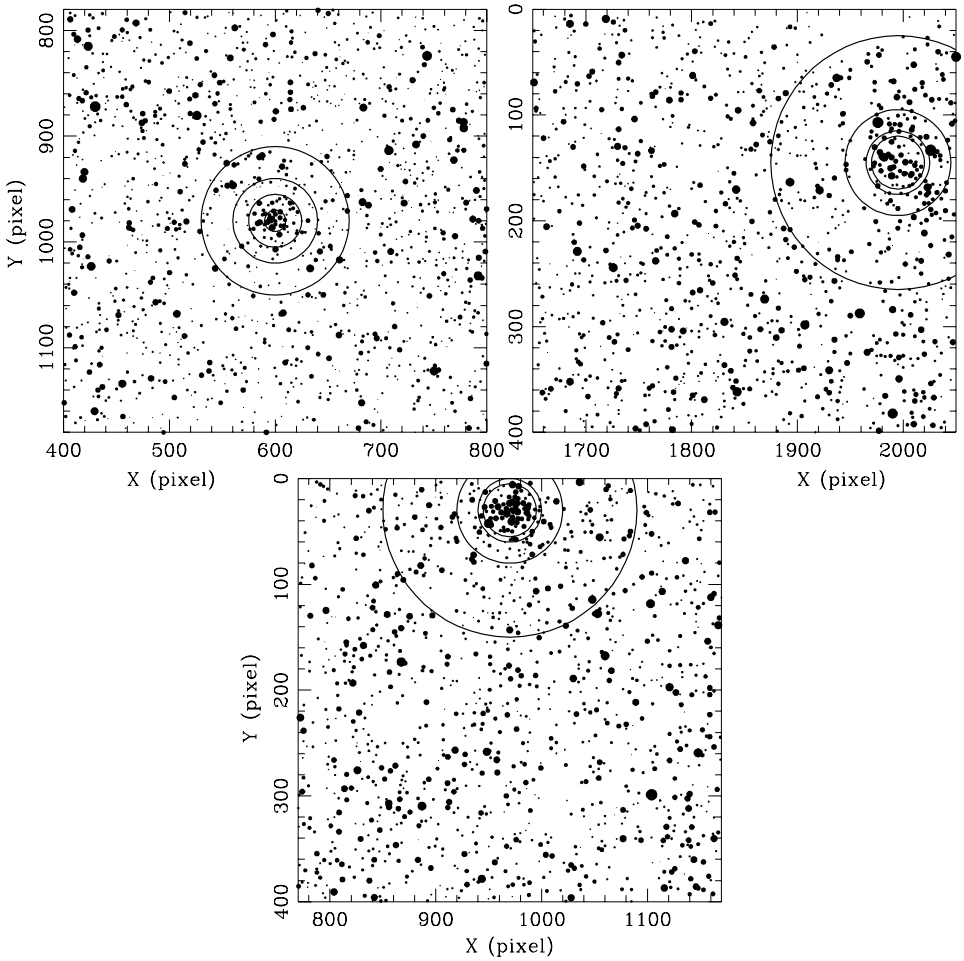

Figure 1 – *continued*

cluster, NGC 1865, was one of these central targets (Geisler et al. 1997), and in the present study its properties are re-addressed for a more detailed analysis. For details on the prescriptions followed for the observation and reduction of these clusters, we refer readers to the work of Geisler et al. (1997).

The six objects have in common the age range 250–700 Myr (Section 4), and they are basically found in two different regions in the LMC. NGC 1836, 1860 and 1865 are projected on the north-west part of the bar region, while SL 444 is also located on the central disc, but outside the bar. LW 224 and SL 548 are both projected on the outer disc. SL 446, another serendipitous cluster (Table 1) projected on the outer disc, is compact and too poorly populated an object to apply the procedures described in Section 3. Consequently, it will not be further discussed in this work. Deeper and higher resolution images would be necessary to derive a useful CMD for SL 446.

3 ANALYSIS OF THE COLOUR–MAGNITUDE DIAGRAMS

When dealing with photometric data that do not provide a membership criterion for individual cluster stars, a worthwhile alternative consists of building CMDs for stars distributed within different regions centred both on the cluster and far away from it as well, in order to separate the fiducial cluster sequence from that of the field. The method requires the knowledge of the cluster central coordinates, the cluster stellar density profile, and the main characteristics of its surrounding field. In the case of relatively small faint clusters projected on crowded fields, the required information can prove to be difficult to obtain. In this sense, a careful analysis of different extracted CMDs can help to disentangle the cluster features from those corresponding to a populous field.

To determine the cluster central positions, we first counted the number of stars distributed along the X and Y directions passing through the clusters and within strips of 200 pixels wide. The width of the strips was fixed so as to sample stars well beyond the clusters and, at the same time, to minimize the number of field stars, which only enhances the background level in the projected star density profiles. Likewise, the counts were done using intervals of 5 and 10 pixels with the purpose of evaluating the influence of the involved spatial resolutions on the determination of cluster centres. Once the projected X and Y distributions were obtained, we performed Gaussian fits using the NGAUSSFIT routine of the STSDAS package. As a first guess for the fits, we fixed the independent term to an arbitrary constant depending on the background levels and the linear term to zero, and left the centre and full width at half-maximum (FWHM) as free parameters. The most important sources of uncertainty in the placement of cluster centres came from the relatively small ratio between the number of cluster and field stars, and the projected intracluster fluctuations due to both cluster and field star density

variations. Cluster centres were finally determined with an accuracy better than three pixels in all cases.

Figs 1(a) and (b) show schematic finding charts with all the stars measured in areas of 2.5 arcmin on a side in the cluster fields. The sizes of the plotting symbols are proportional to the T_1 brightness of the stars. The circles were defined so as to investigate different extracted CMDs. Starting from the cluster centres, we also counted the number of stars distributed in concentric rings five pixels wide. The resulting density profiles are shown in Fig. 2. The latter show the number of stars per unit area expressed in pixels. The vertical straight lines indicate the radii of the circular extractions used to build the respective CMDs. As shown in Fig. 2, clusters are in general very small. Most of their stars lie within circles with radii of ∼30–40 pixels (11.5–15.4 arcsec) and they reach, on average, at their centres stellar densities five times higher than the surrounding fields. In the case of SL 444, the stellar density at its centre is even lower, less than three times that of its field. In general, the outermost radii selected have stellar densities that are still slightly above the background level.

Fig. 3. shows an example of the resulting set of extracted T_1 versus $C–T_1$ CMDs, for stars in the area of NGC 1865. The figure contains separate panels for four different circular extractions which are labelled in pixels at the top-left margins. The smallest circular extractions were used to isolate a predominant number of cluster stars in comparison to field stars. They consist of very small areas given the generally small size of the clusters (see Fig. 2). Certainly, the innermost extracted CMDs do not contain the whole cluster stellar population, but minimize the influence of field stars on their fiducial sequences. The most representative surrounding field CMDs are those built from the most external circular extractions, whose delimiting circles were not drawn in Figs 1(a) and (b) because they encompass larger areas. These areas were chosen to lie well beyond the visible extent of the clusters. Finally, two extracted CMDs between the innermost and outermost CMDs were also included in Fig. 3, in order to show the transition from dominate cluster star to field star CMDs. The choice of the various radii for each cluster was an iterative, slightly subjective process designed to obtain the best representation of the cluster and its transition to the field. In the case of NGC 1836, the $30 < r < 60$ pixel CMD resulted in a better definition of the fiducial cluster sequences, with a main sequence (MS) approximately one magnitude deeper than the $r < 30$ pixel CMD due to the increasing crowding in the smallest circular extraction. In addition, we defined two circular extractions for BRHT4b given its proximity in the sky to NGC 1836 (see Fig. 1a), whose CMD is very different (Piatti et al. 2003). We excluded from the $100 < r < 120$ pixel CMD of NGC 1836 any star within 35 pixels of BRHT4b.

We estimated that the contamination of field stars in the extracted CMDs adjacent to the innermost ones varies between 40 and 75 per cent, with the exception of LW 224 in which the field contamination only reaches 25 per cent. The innermost extracted CMD of LW 224 is better defined. The increasing presence of field stars in the CMDs adjacent to those of the smallest circular extractions is mainly due to field MS stars, which superimpose on the cluster MSs at their faintest portions, or extend the cluster MS toward fainter magnitudes. For this reason, in the subsequent analysis we used the

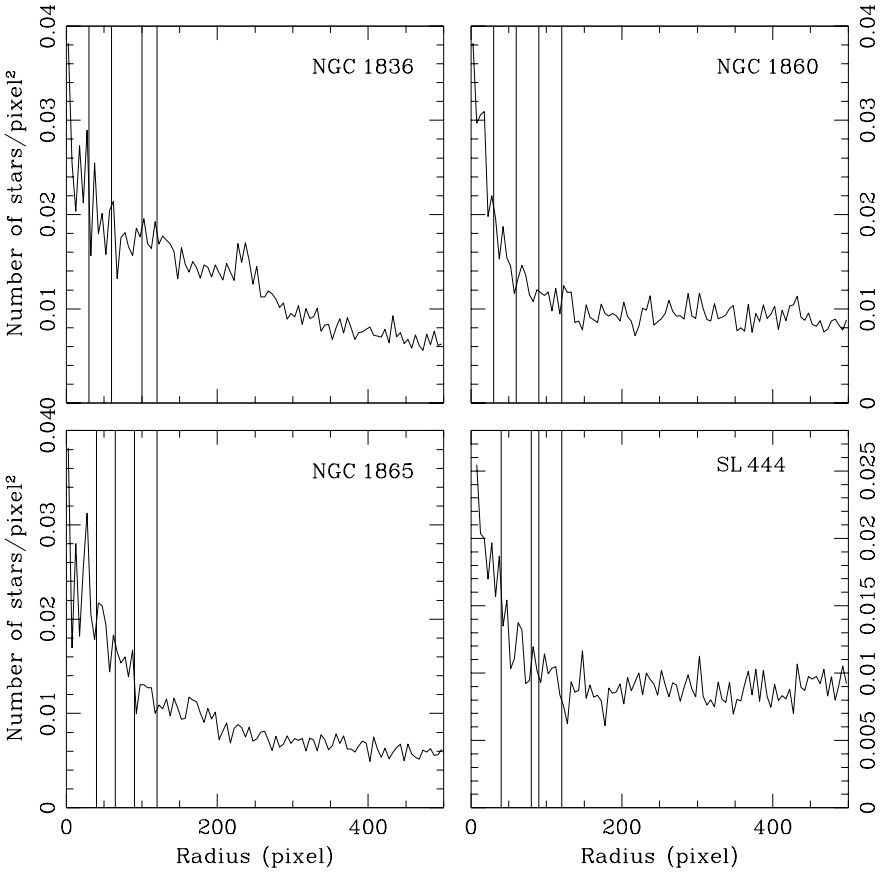

Figure 2. Density profiles for the selected clusters. Vertical straight lines indicate radii of the circular extractions used in the corresponding CMDs (see Section 3).

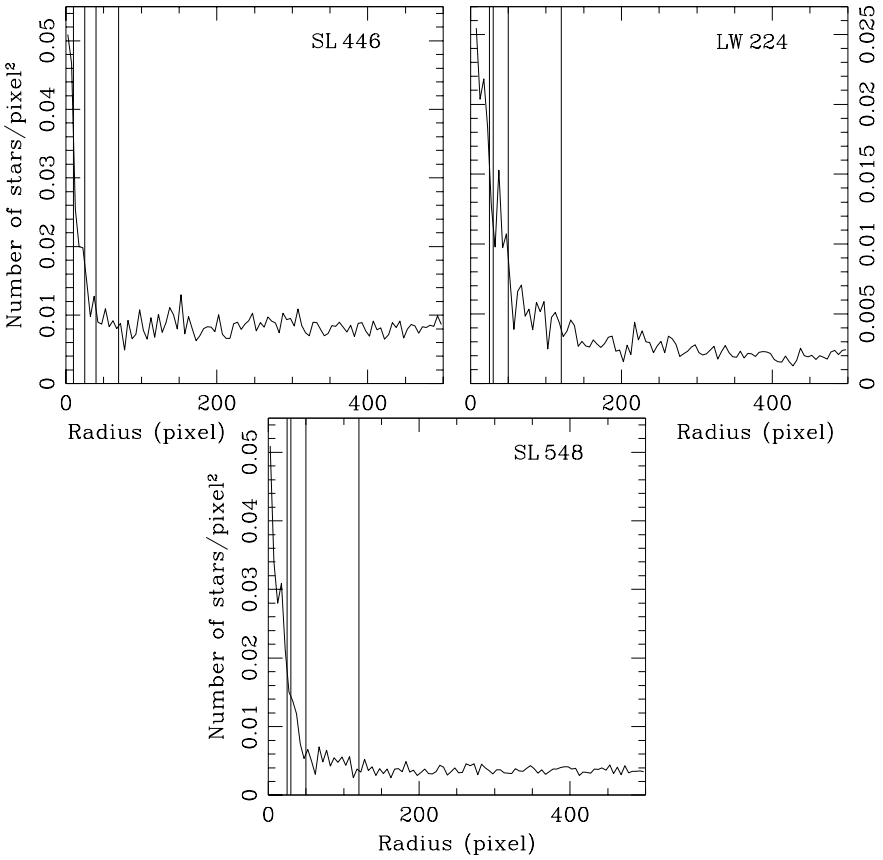

Figure 2 – *continued*

innermost extracted CMDs for the relatively sharp density profile clusters SL 444, LW 224 and SL 548, and the second extracted CMDs for NGC 1836, 1860 and 1865 as cluster CMDs. For NGC 1865 and LW 224, we added to the respective selected extracted CMDs red giant branch stars which appear in the corresponding adjacent outer extracted CMDs in order to better determine cluster parameters.

4 CLUSTER FUNDAMENTAL PARAMETERS

To estimate cluster ages and metallicities from the extracted CMDs, we used theoretical isochrones computed for the absolute M_{T_1} versus $(C–T_1)_o$ plane. Recently, Lejeune & Schaerer (2001) and Girardi et al. (2002) calculated theoretical isochrones for the Washington photometric system, independently. Lejeune & Schaerer used a library of synthetic stellar spectra (Lejeune, Cuisinier & Buser 1997, 1998; Westera, Lejeune & Buser 1999) to calculate synthetic photometry for the entire set of the Geneva stellar evolutionary models, and hence to obtain the corresponding isochrones. The theoretical isochrones provided by Girardi et al. (2002) were computed from a rewritten formalism for converting synthetic stellar spectra into tables of bolometric corrections, assuming that Vega has magnitude 0.03 in all the Washington filters. Fig. 4 shows a comparison between both sets of isochrones for the age and metallicity ranges of our cluster sample, which were computed by using the mentioned basic precepts and taking into account overshooting effects. As can be seen, there are no significant differences in the shape of the MSs nor in the positions of the MS turn-offs and red giant clumps, and the agreement is very satisfactory. For the sake of uniformity with previous studies (Piatti et al. 2002; Geisler et al. 2003; Piatti et al. 2003), we decided to use the set of isochrones of Lejeune & Schaerer (2001).

To enter these isochrones in the observed CMDs, the cluster reddenings and the LMC distance modulus are needed. For the LMC distance modulus, we adopted the value $(m - M)_o = 18.50 \pm 0.10$, obtained from a consensus of recent studies based on the K-band magnitude of the red clump (Alves et al. 2002; Pietrzynski & Gieren 2002; Sarajedini et al. 2002). We used the extinction maps built by Burstein & Heiles (1982, hereafter BH) to derive cluster reddening estimates. BH maps provided us with foreground $E(B–V)_{BH}$ colour excesses as measured from the H I (21-cm) emission data. More recently, Schlegel, Finkbeiner & Davis (1998, hereafter SFD) provided full-sky maps based on the 100-μm dust emission. However, we decided not to use SFD's maps because they are basically saturated towards the inner parts of the LMC disc. Nevertheless, for the farthest cluster of the sample from the LMC centre (SL 548) the SFD reddening is the same as that of BH, which shows that differential reddening does not exist in the LMC along the line of sight of the observed clusters. The resulting interpolated $E(B–V)_{BH}$ values are listed in column 2 of Table 2.

Cluster ages were then determined from averaging the ages of the isochrones which most resemble the cluster MSs and best match MS turn-offs and red giant clumps. In the matching procedure, we commonly employed four different isochrones with three distinct metallicities each; isochrones ranging from slightly younger to slightly older than the derived cluster age. Fig. 5 shows the results of the fittings. For each cluster we plot two different isochrones with ages

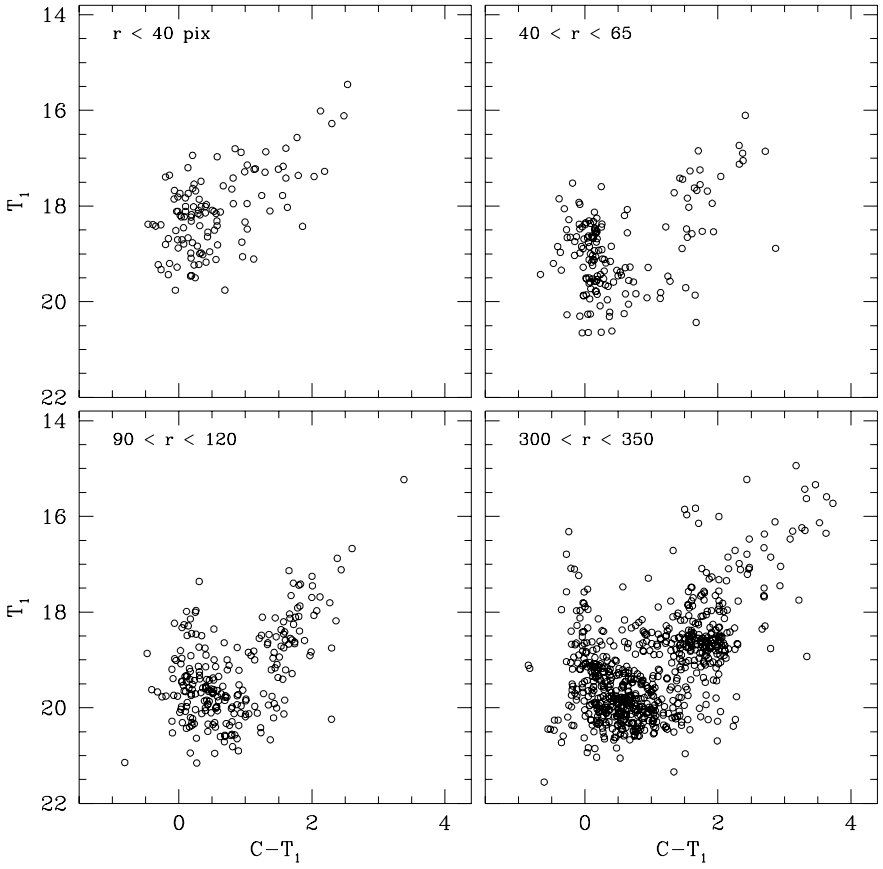

Figure 3. Washington T_1 versus $C–T_1$ CMDs of stars in the field of NGC 1865. Extraction radius in pixels is given in each panel.

and metallicities bracketing the derived value. We note that the appreciable separation in $C–T_1$ colours from the MS up to red giant phases between isochrones of the same age and different metallicity graphically illustrates the competitive metallicity sensitivity of this Washington index. The final cluster ages and metallicities along with their estimated uncertainties are successively listed in columns 3 and 4 of Table 2.

We similarly estimated the representative age and metallicity of the surrounding field of NGC 1860 and 1865 (both clusters were observed within the same CCD field), by employing the δT_1 index and theoretical isochrones. δT_1, the difference in magnitude between the mean magnitude of the giant clump/horizontal branch and the MS turn-off, was calibrated by Geisler et al. (1997) in terms of age for clusters older than 1 Gyr. To measure δT_1 we took into account the MS with the turn-off containing the largest number of stars because the field CMD is composed of MSs of different stellar populations. Using the resulting giant clump and MS turn-off T_1 magnitudes as references, we fitted theoretical isochrones of Lejeune & Schaerer (2001) in order to estimate the representative field metallicity. Surrounding field stars were defined as those stars distributed within a region delimited by an inner circle centred on the cluster with a radius three times bigger than that of the cluster and extending to the boundary of the CCD field. For this purpose, we defined the radius of a cluster as the distance from its centre at which the number of stars per arcmin^2 above the background level is greater than $4 \times \sigma_{\rm back}$, where $\sigma_{\rm back}$ represents the standard deviation of the star density in the surrounding field. We obtained a surrounding field metallicity of [Fe/H] $= -0.4 \pm 0.2$ (isochrone of $\log t = 8.9$), and $\delta T_1 = 0.4 \pm 0.1$ which corresponds to an age of $t = 0.9 \pm 0.2$ Gyr (age obtained by extrapolating the calibration of Geisler et al. 1997). More details on the procedure used to estimate surrounding field ages and metallicities are described by Geisler et al. (2003), who also derived the ages and metallicities of the surrounding fields of the remaining clusters of the sample. We point out that this age corresponds to the well-populated youngest turn-off of the field red stellar population.

5 DISCUSSION

The 36-arcsec separation between NGC 1836 and BRHT4b is closer than the maximum separation of 1.4 arcmin adopted as a selection criterion in the new catalogue by Dieball, Müller & Grebel (2002), which includes all binary and multiple cluster candidates. Dieball et al. (2002) gave evidence that between 56 per cent (bar region) and 12 per cent (outer LMC) of the detected pairs can be explained statistically. They used the Bica et al. (1999) catalogue of 6659 objects, including star clusters, emission-free associations and objects related to emission nebulae, as the foundation of their work. As NGC 1836 and BRHT4b have different ages (400 versus 100 Myr), these two clusters were probably not formed in the same giant molecular cloud. For the close pair of SL 385 and SL 387, Dieball & Grebel (2000) arrived at the same conclusion deriving a projected distance of 45.6 arcsec, and an age difference of $\Delta t \geqslant 80$ Myr. We consider that chance superpositions or an encounter of two clusters with different origins might explain the proximity of NGC 1836 and BRHT4b, located in the north-west edge of the densely populated bar region.

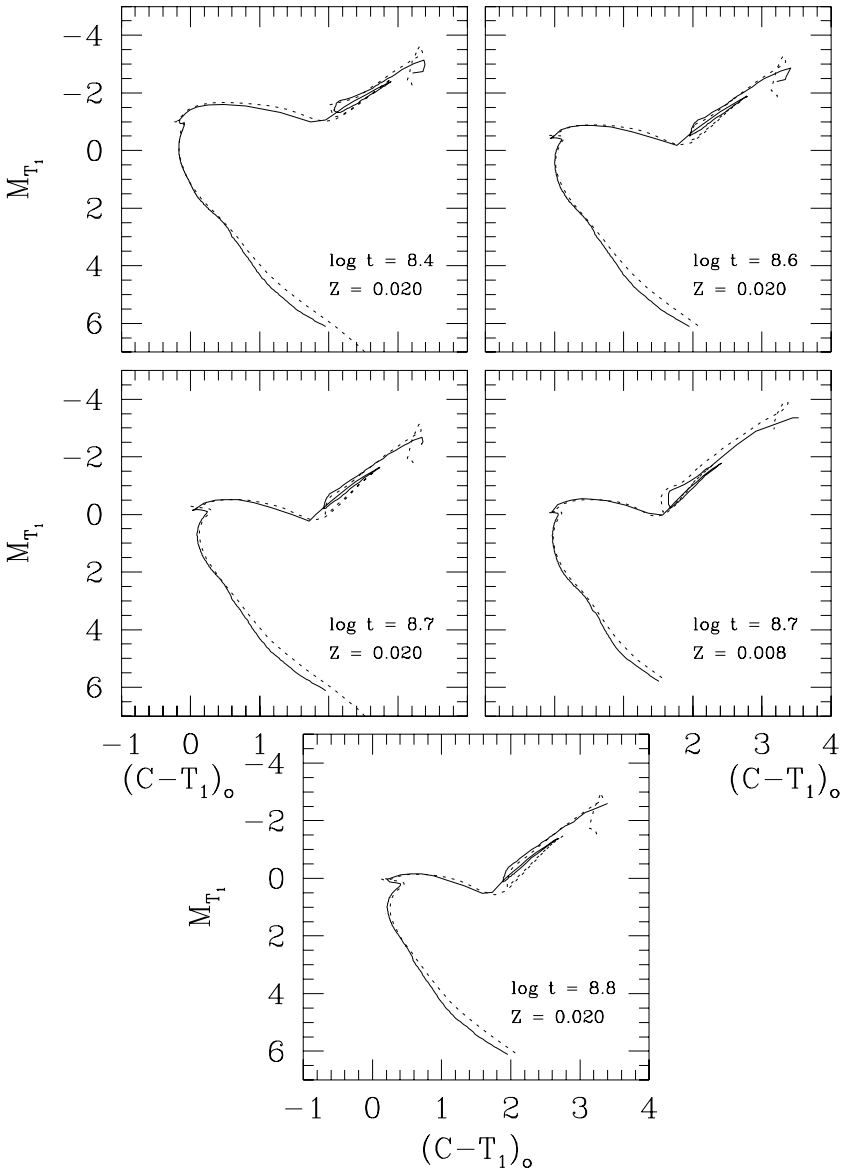

Figure 4. Comparison between theoretical isochrones computed by Lejeune & Schaerer (2001, solid lines) and Girardi et al. (2002, dotted lines) for ages and metallicities of the cluster sample.

Table 2. Fundamental parameters of the LMC cluster sample.

Name	$E(B-V)_{BH}$	Isochrone age (Myr)	Isochrone [Fe/H]	R (°)
NGC 1836	0.06	400±100	0.0±0.2	2.3
NGC 1860	0.08	250±50	0.0±0.2	1.6
NGC 1865	0.06	500±100	−0.2±0.2	1.5
SL 444	0.06	500±100	−0.4±0.2	2.1
LW 224	0.06	700±200	0.0±0.2	3.5
SL 548	0.08	400±100	0.0±0.2	3.6

To investigate the chemical evolution of the LMC from the lower age limit of the LMC age gap (∼3 Gyr) until the present, we added the studied clusters to a list of selected LMC clusters. The selection was performed in order to generate a cluster sample with ages and metallicities determined on the same scale as the present cluster sample; see also Geisler et al. (2003) for a detailed description of these scales. This avoids uncertain fundamental parameter determinations and zero-point offsets between different age and/or metallicity scales. We included those clusters observed by Bica et al. (1998), Piatti et al. (1999), Piatti et al. (2002), Geisler et al. (2003) and Piatti et al. (2003). We also included NGC 2121, which was observed by Piatti et al. (2002) along with NGC 2155 and SL 896 (LW 480). Following their steps in the analysis of the CMDs of these two clusters, we obtained for NGC 2121: $\delta T_1 = 1.90 \pm 0.20$, δT_1 age = 2.5 ± 0.5 Gyr, and standard giant branch (SGB) [Fe/H] = -0.65 ± 0.20. By using the Lejeune & Schaerer (2001) isochrones, we estimated the age and metallicity of NGC 2121 as 2.4 ± 0.4 Gyr and -0.5 ± 0.2 dex, respectively. For its surrounding field, we derived $\delta T_1 = 1.80 \pm 0.15$, δT_1 age = 2.3 ± 0.3 Gyr, and SGB [Fe/H] = -0.45 ± 0.2, and from isochrone fitting we obtained the age and metal abundance of 2.7 ± 0.4 Gyr and -0.4 ± 0.2 dex, respectively. All the independent age and metallicity determinations are in very good agreement. Moreover, for 11 clusters with age determinations from isochrones and δT_1 values, we derived $|\Delta(t_{\delta T_1} - t_{\rm isochrone})| = 0.2 \pm 0.2$ Gyr. Thus, we gathered a total of 37 LMC

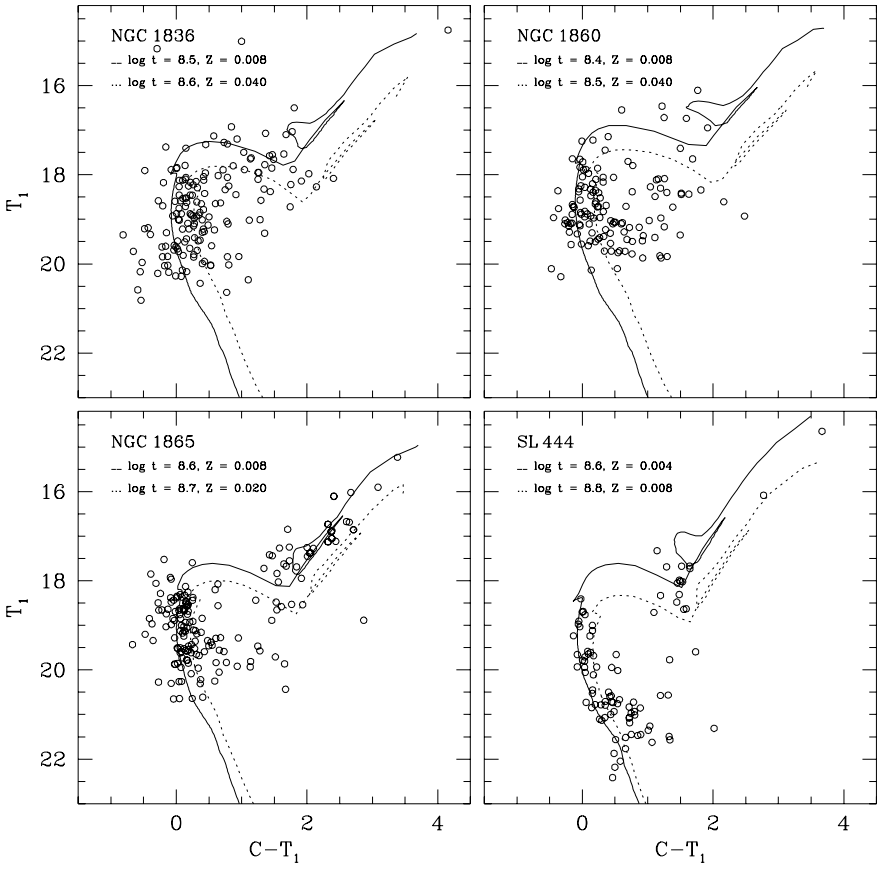

Figure 5. Washington T_1 versus $C–T_1$ CMDs for the clusters. Isochrones from Lejeune & Schaerer (2001), computed taking into account overshooting, are overplotted.

clusters with ages and metallicities determined on a homogeneous scale.

The resulting cluster list given in Table 3 contains objects distributed throughout the LMC disc. We plot in Fig. 6 the relative projected spatial distribution for these selected objects. As the galaxy centre, we adopted the position of NGC 1928 ($\alpha_{2000} = 5^{\rm h}20^{\rm m}57^{\rm s}$, $\delta_{2000} = -69^\circ28'41''$), which is indicated as a cross in the figure. We then divided the sample into outer and inner LMC clusters according to the criterion given by Bica et al. (1998), to whom outer disc clusters are located at deprojected distances larger than 4°, and we represented them, respectively, with open triangles and circles. Fig. 7 (top-left panel) reveals that young clusters are preferentially located (and probably formed) in the inner disc, while intermediate-age clusters (IACs, ages ≈1–<3 Gyr) are mostly spread over the outer disc. This spatial–age distribution is also seen in the age versus relative declination diagram (top-right panel), even though the angular distribution of clusters in this coordinate is about three times smaller than that for right ascension. On the other hand, the relation between cluster and surrounding field ages (bottom panel) shows that clusters and fields have similar (intermediate) ages in the outer disc, whereas the inner LMC disc can contain clusters with different ages, generally smaller than those of their fields, from a couple of tens of millions of years up to ages similar to those of their respective fields. Note that the youngest surrounding fields are placed in the inner LMC disc (open circles) and are 1 Gyr old, which suggests that the most recent strong star-formation events have preferentially taken place in the central body of the LMC at that time. Olsen (1999) derived the star-formation history for six LMC fields from deep *Hubble Space Telescope* (*HST*) CMDs, and also found that the most recent and important peak in the star formation rate occurred at ∼1 Gyr.

Fig. 8 depicts the relationships between cluster positions, cluster metallicities and the metallicity of their surrounding fields. Symbols are the same as in Fig. 6. The different panels show that, on average, inner disc clusters are not only younger than the outer ones but also more metal-rich; some of them even having solar metallicity. In contrast, our IACs have metal abundances lower than [Fe/H] = −0.35 dex. Likewise, inner clusters located to the west of the LMC centre are younger and more metal-rich than their eastern counterparts, which is in agreement with the bar-induced star-formation scenario suggested by Dottori et al. (1996). Least-squares fits to the top-left panels of Figs 7 and 8 for these clusters yielded linear correlation coefficients of $r = 0.9$ and 0.7, respectively. As in the age behaviour between clusters and surrounding fields, IACs and fields appear to share very similar metallicities, while younger clusters and their fields show a larger dispersion around the identity relation. On the other hand, the fact that surrounding fields do not appear to be more metal-rich than [Fe/H] ∼ −0.2 (bottom panel) nor younger than ∼1 Gyr, could also constitute a lower limit to the time and an upper limit to the metal content since the LMC last closely interacted with our Galaxy (van der Marel et al. 2002).

Finally, we analysed the chemical evolution of the clusters and surrounding fields from their age–metallicity and metallicity–deprojected distance relationships, and compared them with those derived from theoretical models. Fig. 9 shows the resulting age–metallicity relation (AMR), wherein filled circles and triangles

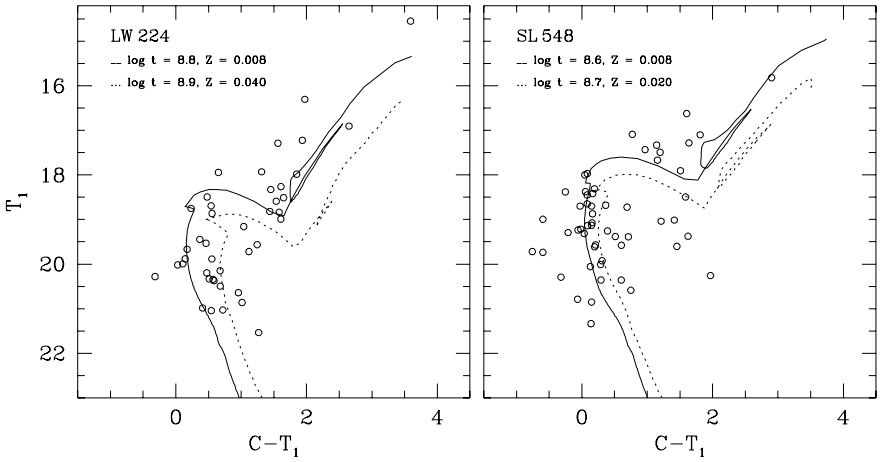

Figure 5 – *continued*

Table 3. Fundamental parameters for additional LMC clusters.

Name	α_{2000} (h m s)	δ_{2000} (° ′ ″)	Age$_{\rm cluster}$ (Myr)	[Fe/H]$_{\rm cluster}$	Age$_{\rm field}$ (Myr)	[Fe/H]$_{\rm field}$	R (°)
SL 8	4 38 00	−69 07 37	1800	−0.40	2000	−0.30	4.8
SL 126	4 56 53	−62 36 37	2200	−0.45	2500	−0.50	9.8
SL 218	5 05 24	−68 30 00	50	−0.40	1300	−0.25	2.4
BRHT4b	5 05 40	−68 38 22	100	−0.40	1300	−0.25	2.2
NGC 1839	5 06 02	−68 37 36	125	−0.40	1300	−0.25	2.2
NGC 1838	5 06 07	−68 26 42	100	−0.40	1300	−0.25	2.4
SL 244	5 07 37	−68 32 31	1200	−0.40	1300	−0.25	2.1
SL 262	5 08 52	−62 26 27	2100	−0.50	2000	−0.45	9.1
NGC 1863	5 11 39	−68 43 48	50	−0.40	900	−0.40	1.6
SL 359	5 17 49	−68 28 22	1600	−0.20	1600	−0.25	1.4
SL 388	5 19 44	−63 31 44	2200	−0.65	2000	−0.55	7.2
SL 446A	5 24 28	−67 43 43	2200	−0.70	3900	−0.75	2.0
SL 437	5 24 47	−75 29 26	1000	–	2000	−0.65	7.3
SL 451	5 25 57	−75 36 33	2200	−0.70	2000	–	7.5
SL 505	5 28 50	−71 37 58	900	−0.40	1300	−0.15	2.9
SL 509	5 29 29	−63 41 11	1200	−0.65	1500	−0.35	6.6
SL 515	5 30 09	−63 25 39	1600	–	–	–	6.9
SL 555	5 31 42	−72 08 46	1900	−0.70	2300	−0.40	3.7
SL 549	5 32 03	−64 14 32	1700	−0.70	2500	−0.70	5.9
SL 674	5 43 20	−66 15 44	2300	−1.00	2800	−0.75	3.9
SL 678	5 43 35	−66 12 31	1500	−0.70	2800	−0.75	3.9
SL 769	5 53 54	−70 04 44	1800	−0.35	–	−0.45	3.9
NGC 2155	5 58 33	−65 28 37	3600	−0.80	3000	−0.75	5.4
SL 817	6 01 09	−70 04 07	1500	−0.35	2000	−0.65	4.7
SL 842	6 07 53	−62 58 40	2200	−0.60	2500	−0.60	8.0
NGC 2209	6 08 34	−73 50 28	1500	–	–	–	8.0
SL 862	6 14 04	−70 40 45	1800	−0.75	2000	−0.55	6.4
OHSC 33	6 16 33	−73 45 58	1400	−0.80	2000	−0.60	8.6
SL 896	6 29 58	−69 20 01	2300	−0.55	3300	−0.80	7.8
OHSC 37	7 08 01	−69 54 10	2100	−0.60	–	–	12.4

representinner and outer disc clusters while open symbols refer to their respective surrounding fields. We included the closed-box enrichment model (dotted line) computed by Geha et al. (1998) using the star-formation history of Holtzman et al. (1997), the theoretical AMR calculated (for application to the SMC) by Da Costa & Hatzidimitriou (1998) based on a simple closed system with continuous star formation under the assumption of chemical homogeneity (short-dashed line), and the bursting model of Pagel & Tautvaišienė (1998) for the LMC and SMC, depicted with long-dashed and solid lines, respectively. It would appear that a bursting formation mechanism, with an important formation event centred at ∼2.0 Gyr, is a better description of the cluster AMR rather than a closed-box chemical evolution model.

The LMC disc field AMR (open symbols of Fig. 9) shows an important jump to higher values in the metal content at ∼2.5 Gyr, which could be associated with a burst-generated star-formation event, although the sample size is rather small to draw a definitive conclusion. The field star-formation process in the outer disc (open

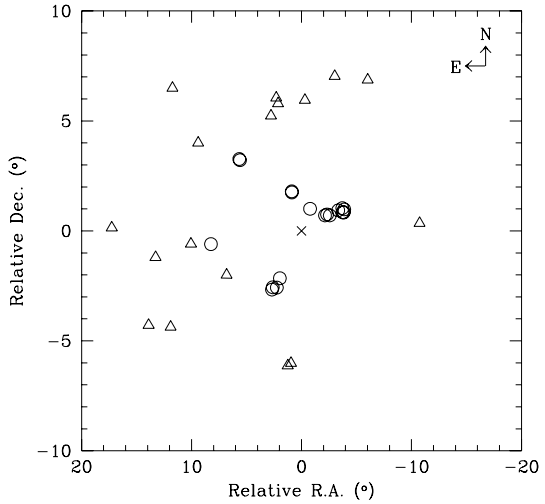

Figure 6. Spatial distribution of LMC clusters in Tables 2 and 3. Circles and triangles represent objects distributed in the inner and the outer LMC discs, respectively. The cross represents the LMC centre.

triangles) appears to have mainly lasted until 2 Gyr ago, while it continued in the inner disc (open circles) for almost 1 Gyr more. When the field star formation ended in the outer disc, the higher metallicity limit was [Fe/H] ~ -0.3, and 1 Gyr later, it was of the order of 0.15 dex more metal-rich in the inner disc. The picture of the cluster AMR is different, although it also appears to repeat the bursting behaviour of the LMC field. Note that outer disc clusters have formed until $\sim$1.0 Gyr ago and reached [Fe/H] values of ~ -0.35, i.e. they were also formed up to $\sim$1.0 Gyr after the most recent outer disc field stars and with similar upper metal abundance limits. In the inner LMC disc until the present time, clusters have been formed at higher metallicities, and some of them even with abundances that reach solar values. Of course, the age we derived for each field is only representative of the range of ages and cluster formation must be accompanied by field star formation.

Fig. 10 reveals some hints for a metallicity gradient in the LMC disc. The upper-left panel shows that younger clusters have predominantly formed in the inner disc within a reasonably wide metal abundance range (Δ[Fe/H] $\approx$ 0.4 dex), while NGC 2155 (age = 3.6 Gyr) is so far the oldest known IAC (bottom-right panel), and has a very low metallicity ([Fe/H] = -0.8 dex). During the

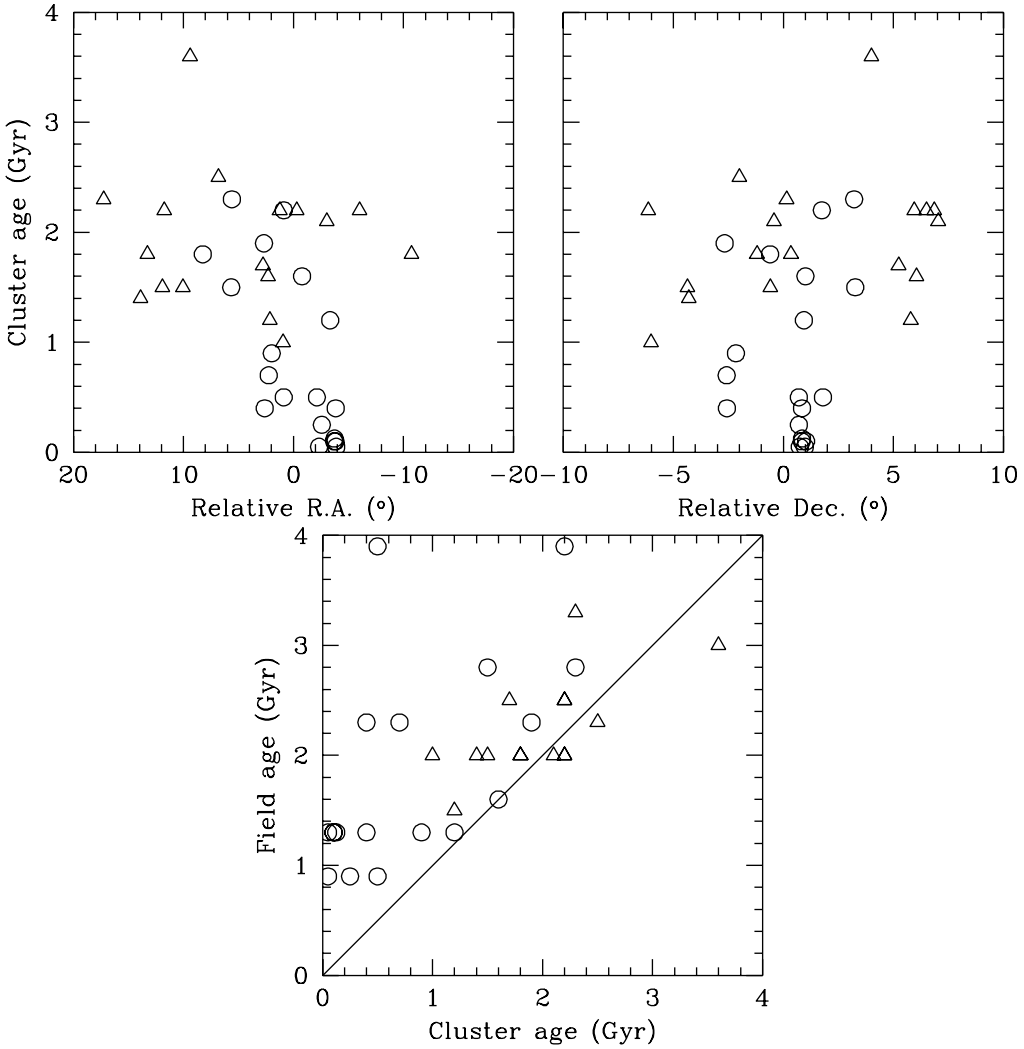

Figure 7. Relationship between the position of clusters in the sky, the cluster ages, and the ages of their surrounding fields. Symbols are the same as in Fig. 6. The solid line in the bottom panel corresponds to the same age for clusters and surrounding fields. Typical age error bar is 10–20 per cent of the age value.

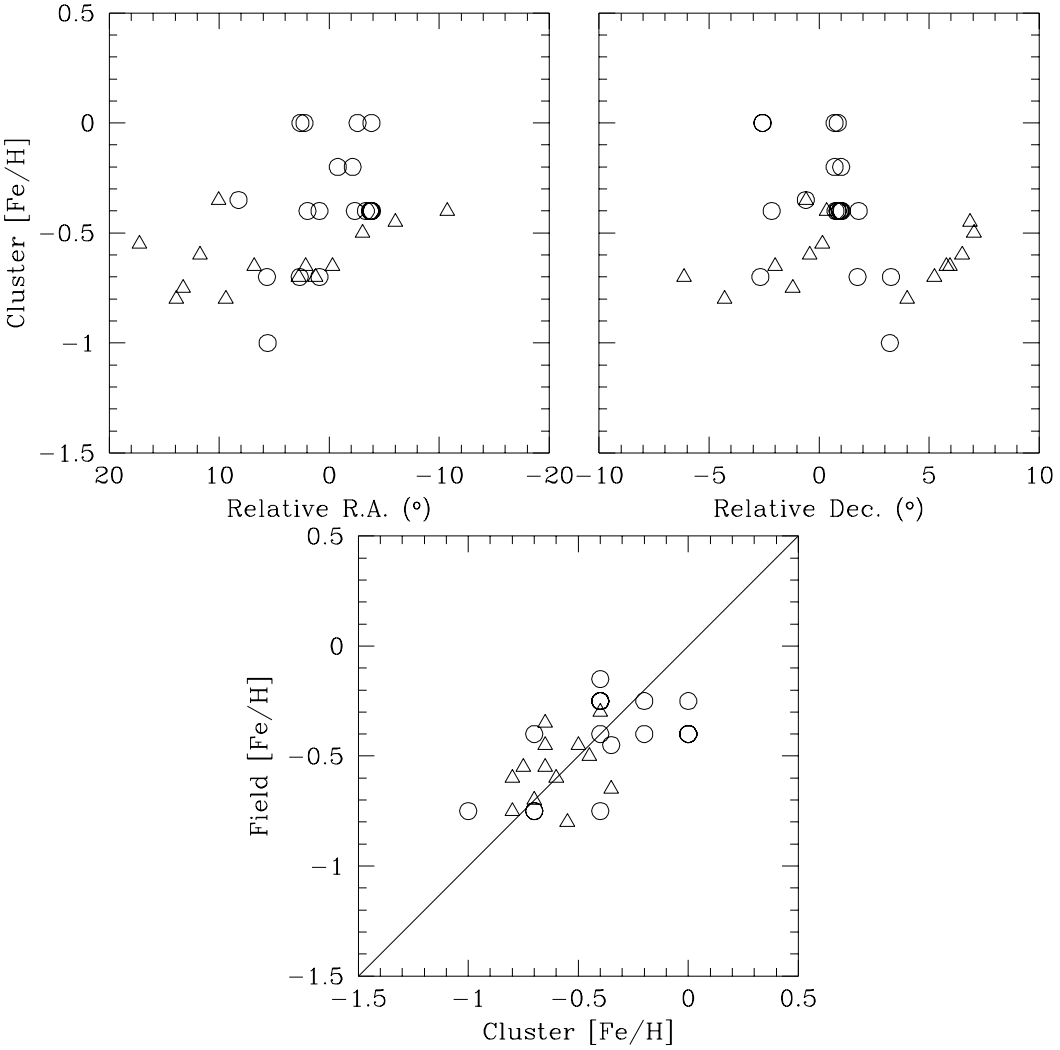

Figure 8. Relationship between the position of clusters in the sky, the cluster metallicities and the metallicities of their surrounding fields. Symbols are the same as in Fig. 6. The solid line in the bottom panel corresponds to the same metallicity for clusters and surrounding fields. Metallicity error bar is ±0.2 dex.

bursting star-formation process which occurred between 2 and 2.5 Gyr ago (bottom-left panel), remarkably metal-poor IACs were formed throughout the whole LMC disc ($\langle$[Fe/H]$\rangle \approx -0.7$), and once the burst had mostly ended (top-right panel), IACs with metallicities $\gtrsim$0.3 dex higher were also formed. Metal-poor and metal-rich IACs seem to have been formed at relatively distinct deprojected distances (R), in the sense that the more distant the cluster, the more deficient its metal content.

6 CONCLUDING REMARKS

The present study deals with Washington photometry of six LMC clusters in the range 250–700 Myr. We derive ages and metallicities and combine them with similar results we have derived homogeneously for 31 additional young or intermediate age clusters in our previous studies. We analyse NGC 1836, 1860 and 1865 which are projected on the bar, SL 444 also located on the central disc but outside the bar, and finally LW 224 and SL 548 in the outer disc.

We employ the total set of 37 clusters and fields to probe the chemical enrichment of the LMC and its spatial distribution. Inner disc clusters are not younger on average than the outer ones but also more metal-rich, some with solar metallicity. In contrast, all but one studied IAC have metal abundances lower than [Fe/H] = −0.35 dex. Inner clusters located to the west of the LMC centre are also younger and more metal-rich than their eastern counterparts. IACs and their surrounding fields appear to share similar metallicities, while for younger clusters a larger dispersion around the identity relation is shown. The studied surrounding fields turned out to be more-metal poor than [Fe/H] ∼ −0.2 and older than 1 Gyr. These values could serve as reference for the lower limit of the time and the upper limit of the metal content since the LMC last closely interacted with our Galaxy.

The chemical evolution of the clusters and surrounding fields from their age–metallicity and metallicity–deprojected distance relationships were compared with those derived from theoretical models. Specifically, the resulting AMR was compared to a closed-box enrichment model computed by Geha et al. (1998) using the star-formation history of Holtzman et al. (1997), the theoretical AMR calculated by Da Costa & Hatzidimitriou (1998) based on a simple closed system with continuous star formation under the assumption of chemical homogeneity, and the bursting models of Pagel & Tautvaišienė (1998) for the LMC and SMC. The results

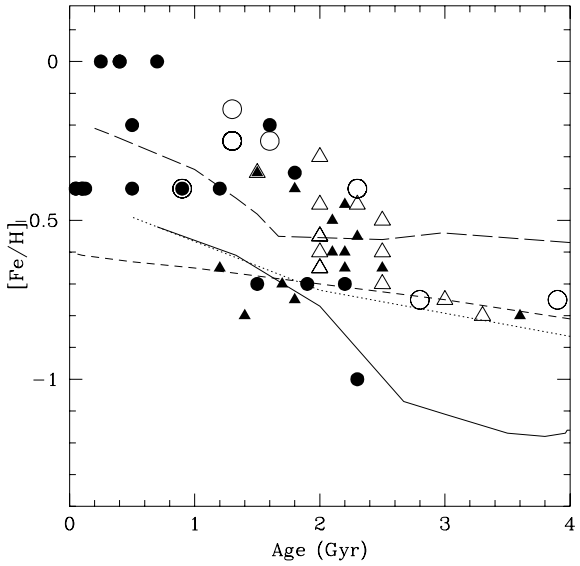

Figure 9. AMR for selected star clusters in the LMC. Filled circles and triangles represent inner and outer disc clusters, respectively, while open symbols refer to their respective surrounding fields (see Section 5 for details). The data are compared with the closed-box models (dotted and short-dashed lines) computed by Geha et al. (1998) and Da Costa & Hatzidimitriou (1998), respectively, and the bursting models for the LMC (long-dashed line) and the SMC (solid lines) of Pagel & Tautvaišienė (1998).

suggest that a bursting formation mechanism, with an important formation event centred at ∼2.0 Gyr, is a better description of the cluster AMR than a closed-box chemical evolution model.

The LMC disc field AMR shows an important jump to higher values in the metal content at ∼2.5 Gyr, possibly related to a burst of star formation. The field star-formation process in the outer disc appears to have lasted until 2 Gyr ago, while it continued in the inner disc for almost 1 Gyr more. The inner disc has been forming clusters more metal-rich than the outer disc, which is a reflection of the AMR, although some hints for an abundance gradient were found for IACs formed 1–2 Gyr ago.

ACKNOWLEDGMENTS

We thank the staff at the Cerro Tololo Inter-American Observatory (CTIO) for the hospitality and assistance during the observations. We also thank the referee Dr David Zurek for his valuable comments. This work was partially supported by the Brazilian institutions CNPq and FINEP, and the Argentinian institutions Agencia Nacional de Promoción Científica y Tecnológica, CONICET and SECYT (Universidad Nacional de Córdoba) and Agencia Córdoba Ciencia. This work is based on observations made at CTIO, which is operated by AURA, Inc., under cooperative agreement with the NSF. DG gratefully acknowledges support from the Chilean *Centro de Astrofísica* FONDAP No 15010003.

REFERENCES

Alves D. R., Rejkuba M., Minniti D., Cook K. H., 2002, ApJ, 573, L51
Bhatia R. K., Read M. A., Tritton S., Hatzidimitriou D., 1991, A&AS, 87, 335
Bica E., Geisler D., Dottori H., Clariá J. J., Piatti A. E., Santos J. F. C., Jr., 1998, AJ, 116, 723
Bica E., Schmitt H. E., Dutra C. M., Oliveira H. L., 1999, AJ, 117, 238
Burstein D., Heiles C., 1982, AJ, 87, 1165 (BH)

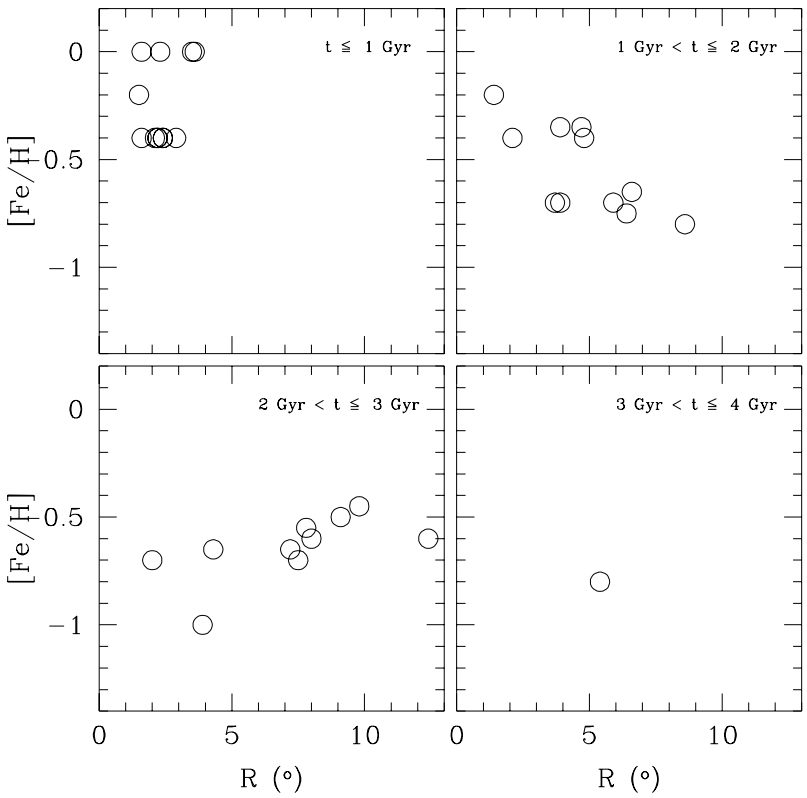

Figure 10. Metallicity versus deprojected radius from the centre of the LMC for the selected cluster sample at different age intervals.

Da Costa G. S., Hatzidimitriou D., 1998, AJ, 115, 1934
Dieball A., Grebel E., 2000, A&A, 358, 897
Dieball A., Müller H., Grebel E., 2002, A&A, 391, 547
Dottori H., Bica E., Clariá J. J., Puerari I., 1996, ApJ, 461, 742
Geha M. C. et al., 1998, AJ, 115, 1045
Geisler D., Bica E., Dottori H., Clariá J. J., Piatti A. E., Santos J. F. C., Jr., 1997, AJ, 114, 1920
Geisler D., Piatti A. E., Bica E., Clariá J. J., 2003, MNRAS, 341, 771
Girardi L., Bertelli G., Bressan A., Chiosi C., Groenewegen M. A. T., Marigo P., Salasnich B., Weiss A., 2002, A&A, 391, 195
Holtzman J. A. et al., 1997, AJ, 113, 656
Ibata R. A., Gilmore G., Irwin M. J., 1994, Nat, 359, 806
Kontizas M., Morgan D. H., Hatzidimitriou D., Kontizas E., 1990, A&AS, 84, 527
Lauberts A., 1982, The ESO/Uppsala Survey of the ESO (B) Atlas. European Southern Observatory, Garching bei Munchen
Lejeune T., Schaerer D., 2001, A&A, 366, 538
Lejeune T., Cuisinier F., Buser R., 1997, A&AS, 125, 246
Lejeune T., Cuisinier F., Buser R., 1998, A&A, 287, 803
Lyngå G., Westerlund B. E., 1963, MNRAS, 127, 31L
Mateo M., 1998, Ann. Rev. A&A, 36, 435
Olsen K. A. G., 1999, AJ, 117, 2244
Pagel B. E. J., Tautvaišienė G., 1998, MNRAS, 299, 535
Piatti A. E., Geisler D., Bica E., Clariá J. J., Santos J. F. C., Jr., Sarajedini A., Dottori H., 1999, AJ, 118, 2865
Piatti A. E., Sarajedini A., Geisler D., Bica E., Clariá J. J., 2002, MNRAS, 329, 556
Piatti A. E., Geisler D., Bica E., Clariá J. J., 2003, MNRAS, 343, 851
Pietrzynski G., Gieren W., 2002, AJ, 124, 2633
Rich R. M., Shara M. M., Zurek D., 2001, AJ, 122, 842
Sarajedini A., Grocholski A. J., Levine J., Lada E., 2002, AJ, 124, 2625
Schlegel D. J., Finkbeiner D. P., Davis M., 1998, ApJ, 500, 525 (SFD)
Shapley H., Lindsay E. M., 1963, Irish, AJ, 6, 74
van der Marel R. P., Alves D. R., Hardy E., Suntzeff N. B., 2002, AJ, 124, 2639
Westera P., Lejeune T., Buser R., 1999, in Hubery I., Heap S., Cornett R., eds, ASP Conf. Ser. Vol. 192, Spectrophotometric Dating of Stars and Galaxies. Astron. Soc. Pac., San Francisco, p. 203

This paper has been typeset from a TEX/LATEX file prepared by the author.